Nanoscale

PAPER

View Article Online
View Journal | View Issue

Cite this: *Nanoscale*, 2015, **7**, 14476

Enhanced photovoltaic performances of graphene/Si solar cells by insertion of a MoS_2 thin film†

Yuka Tsuboi,[a] Feijiu Wang,[a] Daichi Kozawa,[a] Kazuma Funahashi,[b] Shinichiro Mouri,[a] Yuhei Miyauchi,[a] Taishi Takenobu[b] and Kazunari Matsuda*[a]

Received 9th May 2015,
Accepted 16th July 2015

DOI: 10.1039/c5nr03046c

www.rsc.org/nanoscale

Transition-metal dichalcogenides exhibit great potential as active materials in optoelectronic devices because of their characteristic band structure. Here, we demonstrated that the photovoltaic performances of graphene/Si Schottky junction solar cells were significantly improved by inserting a chemical vapor deposition (CVD)-grown, large MoS_2 thin-film layer. This layer functions as an effective electron-blocking/hole-transporting layer. We also demonstrated that the photovoltaic properties are enhanced with the increasing number of graphene layers and the decreasing thickness of the MoS_2 layer. A high photovoltaic conversion efficiency of 11.1% was achieved with the optimized trilayer-graphene/MoS_2/*n*-Si solar cell.

Introduction

With an increase in low dimensional material research, atomically thin materials have been widely and intensively studied from the viewpoints of both fundamental physics and applications.[1–8] Transition-metal dichalcogenides (TMDs) (MX_2; M = Mo, W; X = Se, S) are among the most attractive two-dimensional (2D) layered materials that can be thinned down to atomic-scale thickness.[9] Monolayer molybdenum disulfide (MoS_2), which is a typical and well-studied TMD system, is a direct bandgap semiconductor, whereas bulk MoS_2 is an indirect bandgap semiconductor. The direct-to-indirect energy-gap transition occurs in MoS_2 when it changes from a monolayer to a bilayer, and the optical bandgap changes from 1.8 eV in monolayer MoS_2 to 1.2 eV in bulk MoS_2.[3,10,11] The optical band gap associated with their energy structures has potential applications in various optical and electronic devices.[12–14]

2D materials are used as building blocks to fabricate artificial multi-junction nanostructures because layered 2D materials can be easily stacked by van der Waals interactions. Artificial multi-junction nanostructures composed of various 2D materials with novel characteristics can be fabricated. Indeed, graphene on h-BN exhibits an extremely high carrier mobility,[15] which is much larger than that of graphene on an SiO_2/Si substrate. Very high photo-responsivity has also been reported for optoelectronic devices based on the stacking of graphene and MoS_2 (graphene/MoS_2).[16–18] The graphene/MoS_2 heterostructure is considered as a promising platform for photovoltaic applications.[19–22] The photovoltaic properties of solar cells based on low dimensional carbon materials and Si heterojunctions have been intensively studied.[23–27] In the case of graphene/Si solar cells, the approaches used to improve the photovoltaic performance have primarily involved carrier doping in the graphene layer, the deposition of an antireflection layer onto the surface of a solar cell, and so on.[28–35]

In this study, we investigate the photovoltaic properties of graphene/MoS_2/n-Si solar cells. The photovoltaic properties were considerably enhanced by the insertion of a large chemical vapor deposition (CVD)-grown MoS_2 thin film, which functions as an effective electron-blocking/hole-transporting layer. The optimized graphene/MoS_2/n-Si solar cell exhibited a high photovoltaic conversion efficiency of 11.1%, which is remarkable conversion efficiency in a photovoltaic device using a MoS_2 thin film. Additionally, the flexibility of the graphene/MoS_2 hetero-structures is quite favorable for the application of this material as carrier transporting/blocking layers in various types of solar cells other than the Si-based ones such as flexible organic and perovskite solar cells. Our findings thus shed light on a new aspect of transition metal dichalcogenide thin films as functional materials for photovoltaics.

Results

Fig. 1(a) shows a schematic of the graphene/MoS_2/n-Si solar cell. It comprises two types of materials, CVD-grown MoS_2 film and graphene, stacked on a patterned n-type SiO_2/Si substrate

[a]*Institute of Advanced Energy, Kyoto University, Gokasho, Uji, Kyoto 611-0011, Japan. E-mail: matsuda@iae.kyoto-u.ac.jp*
[b]*Department of Advanced Science and Engineering, Waseda University, Shinjuku-ku, Tokyo 169-8555, Japan*
†Electronic supplementary information (ESI) available. See DOI: 10.1039/c5nr03046c

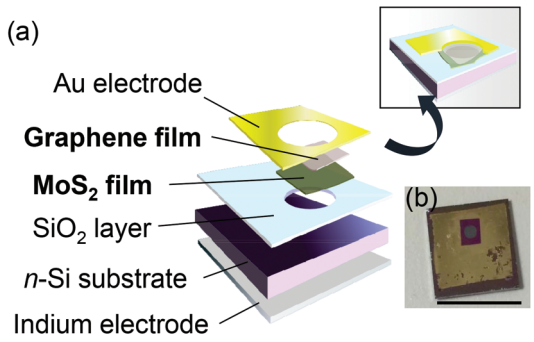

Fig. 1 (a) Schematic of the graphene/MoS_2/n-Si solar cell. (b) An optical image of a graphene/MoS_2 thin film deposited onto a substrate. The scale bar is 1 cm.

(with a ϕ = 1 mm window). Large-scale MoS_2 films for solar cells were fabricated by the CVD method.[36–38] As the first step, an MoO_3 (99.98%, Sigma-Aldrich) film with the desired thickness was fabricated on an SiO_2/Si substrate using the thermal-evaporation technique under vacuum conditions (~10^{-3} Pa); this MoO_3 film was subsequently sulfurized. The sulfurization step of the MoO_3 film was conducted using the CVD furnace. The SiO_2/Si substrate with the MoO_3 film was placed in the center of a quartz tube, and sulfur (>98%, Wako) was loaded at the upstream side. The substrate was heated by the CVD furnace to 750 °C at a heating rate of 15 °C min^{-1} and maintained at this temperature for 30 min. At the growth temperature (750 °C), sulfur was also heated to 190 °C using a ribbon heater, resulting in sulfur transport. All processes were performed under high-purity Ar gas flowing at 50 sccm under ambient conditions. We fabricated MoS_2 films with various thicknesses on SiO_2/Si substrates, as shown in Fig. S1.†

The graphene/MoS_2/n-Si solar cells were fabricated by transferring CVD-grown MoS_2 films and graphene films (single-layer graphene, Graphene Platform) onto the n-type Si substrate (1–5 Ω cm^{-1}) with a SiO_2 layer. A circular window with a diameter of 1 mm was patterned on the SiO_2/Si substrate. This Si substrate was dipped into buffered hydrofluoric acid (HF) solutions for several seconds to remove the natural oxidation layer on the window, which obstructs the electrical contact. The MoS_2 film was then transferred *via* thermal release tape (REVALPHA; No. 3195MS, Nitto Denko). In this study, the transfer process using the thermal release tape was a more facile method compared with the conventional method of using a polymer support film.[39,40] In Fig. S2,† we show the MoS_2 transfer process in detail. For the fine transfer, the first key step is peeling the CVD-grown MoS_2 film from the growth substrate. The water droplet facilitates clear peeling because of the difference in hydrophobicities between the SiO_2/Si substrate and the MoS_2 film.[40] In this transfer method, the process is completed quickly, because the MoS_2 film can be released from the tape by heating, thereby eliminating the need to expose the film to a solution for a prolonged period.

Subsequently, we transferred graphene layers onto MoS_2/n-Si. Poly(bisphenol A carbonate) dissolved in chloroform (3 wt%) was spin-coated onto the single-layer graphene deposited onto copper foil for the transfer process. The graphene film was floated on $FeCl_3$ to etch out the copper foil and was subsequently transferred to the MoS_2/n-Si substrate.[38] The graphene/MoS_2/n-Si was baked at 120 °C for 5 min, and the polymer layer was then dissolved in chloroform. Finally, Au was deposited as an electrode onto the surface of the graphene/MoS_2/n-Si, with the exception of the window region, *via* the Ar-ion sputtering method (Fig. 1(b)). Indium (In), as the cathode, was soldered onto the back side of the solar cell. The process of fabricating the graphene/MoS_2/n-Si solar cell is described in the ESI.†

Fig. 2(a) shows the Raman spectrum of the CVD-grown MoS_2 film. The spectrum shows several Raman peaks, including the in-plane E^1_{2g} mode (~383 cm^{-1}) and the out-of-plane A_{1g} (~408 cm^{-1}) mode of MoS_2. The frequency difference between the E^1_{2g} and A_{1g} Raman peaks (~25 cm^{-1}) is consistent with the previously reported values for bulk MoS_2,[41,42] which suggests that the MoS_2 film used in this study is relatively thick, as described below in detail. The Raman spectrum of the graphene/MoS_2 structures also indicates the vertical stacking of graphene/MoS_2 (see ESI Fig. S3†).

Fig. 2(b) shows the absorption spectrum of the MoS_2 film deposited on the quartz substrate. Distinct absorption peaks around 680 nm and 640 nm are observed in the spectrum,

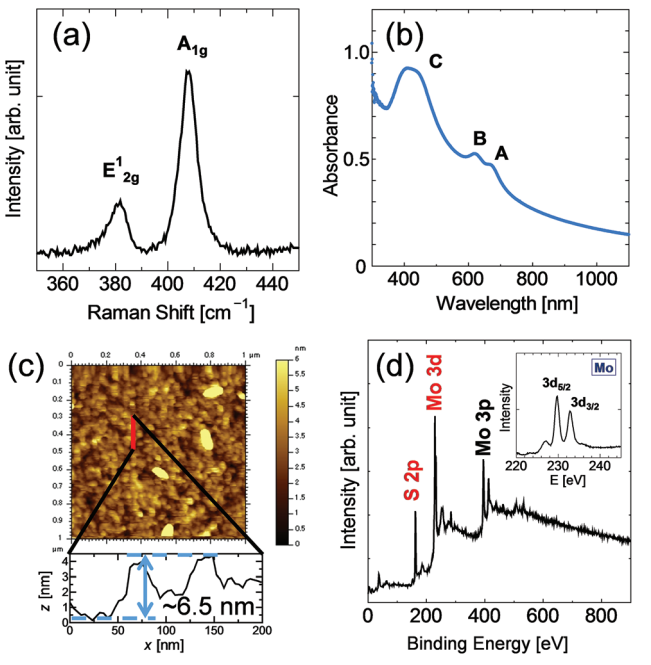

Fig. 2 Characterization of CVD-grown MoS_2 films. (a) Raman spectra of MoS_2 films. The two Raman peaks associated with MoS_2, an in-plane (E^1_{2g}) mode at 383 cm^{-1} and an out-of-plane (A_{1g}) mode at 408 cm^{-1}, are observed. (b) Optical absorption spectra of MoS_2. Distinct absorption peaks associated with A and B excitons are observed. (c) AFM image of an as-grown MoS_2 film. The height profile in the line is shown in the figure. (d) X-ray photoelectron spectrum of the MoS_2 film showing Mo and S peaks. The inset is the Mo 3d spectrum.

which are assigned as A exciton (680 nm) and B exciton (640 nm) peaks associated with the direct bandgap transitions at the *K* point of MoS_2 in the momentum space. Also, we observed the intense C peak at ~460 nm. This peak arises from the distinguishing band structure (band nesting), which is the parallel region of the conduction and valence bands.[20,43,44]

We investigated the thickness of the MoS_2 films using atomic force microscopy (AFM). Fig. S1(c)† shows AFM images measured at the step edge of a typical MoS_2 film used for devices and deposited onto a Si substrate. The inset of Fig. S1(c)† shows the profile at the line in the figure. The thickness of this MoS_2 film was evaluated as ~17 nm on the basis of this height profile, which corresponds to a film with ~20 MoS_2 layers because the thickness of a monolayer of MoS_2 is ~0.7 nm.[45] The evaluated thickness is consistent with the Raman spectral data (Fig. 2(a)) and with the absorption spectra (Fig. 2(b)). Fig. 2(c) shows the surface morphology of MoS_2 films measured by AFM. The surface of CVD-grown MoS_2 films shows the assembly of small grains. In particular, we fabricated MoS_2 films with various thicknesses as shown in Fig. S1(b) and (d).†

We conducted X-ray photoelectron spectroscopy (XPS) of fabricated MoS_2 films to verify the absence of residual ingredients. The XPS spectrum in Fig. 2(d) shows several peaks of the Mo 3d and S 2s core levels. The Mo 3d XPS spectrum is also shown in the inset of Fig. 2(d), which indicates that the peaks at 162.6, 229.8, and 232.8 eV are associated with the S 2s, Mo $3d_{5/2}$, and Mo $3d_{3/2}$ core levels. The binding energies of these peaks are consistent with the previously reported values of Mo^{4+} and S_2^- in MoS_2.[46,47] The Raman, optical absorption, AFM and XPS data, as shown in Fig. 2(a)–(d), certify that MoS_2 films were definitely deposited *via* the CVD method.

Fig. 3(a) shows the current-density–voltage (*J–V*) curves of the monolayer-graphene/MoS_2/n-Si solar cell under dark and AM 1.5 illumination conditions. The *J–V* curve of the monolayer-graphene/MoS_2/n-Si solar cell under the dark conditions (gray line) exhibits typical diode behavior. Furthermore, the monolayer-graphene/MoS_2/n-Si solar cell (yellow line) exhibits clear photovoltaic properties. The open-circuit voltage V_{OC}, short-circuit current density J_{SC}, and fill factor FF of the cell are 0.41 V, 13.1 mA cm^{-2}, and 0.25, respectively, which results in a photovoltaic conversion efficiency (η) of 1.35%. The inset of Fig. 3(a) shows the *J–V* curves of a graphene/n-Si solar cell without a MoS_2 layer, where the fabrication process and materials were the same as those used to fabricate the monolayer-graphene/MoS_2/n-Si cell. The photovoltaic parameters V_{OC}, J_{SC}, and FF are 0.38 V, 6.8 mA cm^{-2}, and 0.17, respectively, which result in a photovoltaic conversion efficiency (η) of 0.44%. All the photovoltaic parameters of the graphene/MoS_2/n-Si solar cell are increased in comparison with those of the graphene/n-Si solar cell in our experiments, which suggests that the MoS_2 layer plays an important role in enhancing the photovoltaic performance of solar cells.

We varied the layer thicknesses of MoS_2 in the graphene/MoS_2/n-Si solar cells. Fig. 3(b) shows the *J–V* curves of graphene/MoS_2/n-Si solar cells with different numbers of graphene layers when illuminated under the AM 1.5 conditions. The red, orange, and yellow lines in Fig. 3(b) correspond to the *J–V* curve of graphene/MoS_2/n-Si solar cells with monolayer, bilayer, and trilayer graphene, respectively, where we controlled the number of graphene layers by changing the number of times the graphene transfer process was conducted. The photovoltaic properties of graphene/MoS_2/n-Si solar cells increased with the increasing number of graphene layers. The trilayer-graphene/MoS_2/n-Si solar cells exhibit a V_{OC}, J_{SC}, and FF of 0.54 V, 28.1 mA cm^{-2}, and 0.53, respectively, which results in a high photovoltaic efficiency of 8.0%.

These parameters of monolayer- and bilayer-graphene/MoS_2/n-Si solar cells and the series resistance estimated from the slope of each *J–V* curve are shown in Table 1 of ESI S4.† The series resistance of the solar cells drastically decreased with the increasing number of graphene layers, and is consistent with the sheet resistance values described in ESI S5† and previously reported results of decreased sheet resistance in graphene layers.[48] The observed sheet resistance 1.5 kΩ per sq. of the tri-graphene layer is low enough to ensure the high efficiency in the graphene/MoS_2/Si solar cell. Our results suggest that the decrease in the series resistance is responsible for the reduction of loss, which contributes to the enhancement of photovoltaic conversion efficiency in graphene/MoS_2/n-Si solar cells.

The incident photon to current conversion efficiency (IPCE) spectra revealed that MoS_2 functions as a shading layer at the point of light absorption, as shown in ESI S5,† and the graphene layers function as semi-transparent conducting layers as shown in Fig. S4.† Thus, the generated carriers in the n-Si layer are the main contributors to the photovoltaic current in the cell. Therefore, the enhancement of photovoltaic performance by the insertion of a MoS_2 layer as shown in Fig. 3(a) implies that the MoS_2 layer plays a positive role as an effective

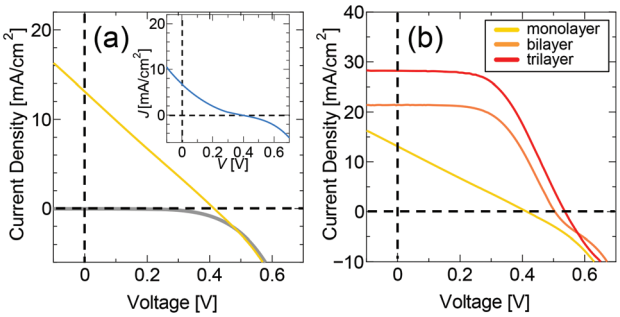

Fig. 3 Photovoltaic performance of monolayer-, bilayer-, and trilayer-graphene/MoS_2/n-Si solar cells. (a) Current density–voltage (*J–V*) curves of a monolayer-graphene/MoS_2/n-Si solar cell under dark (gray line) and under AM 1.5 illumination conditions (yellow line). The *J–V* curve of a monolayer-graphene/n-Si solar cell under AM 1.5 illumination is also shown in the inset. (b) *J–V* curves of monolayer-, bilayer-, and trilayer-graphene/MoS_2/n-Si solar cells, where the number of graphene layers was controlled by the number of graphene transfer processes performed. The thickness of the MoS_2 film was ~17 nm.

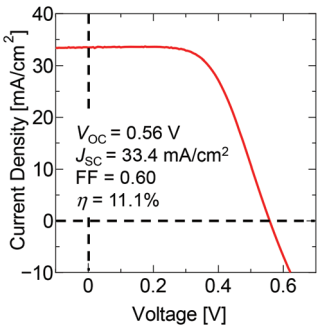

Fig. 4 The current density–voltage (J–V) curves of a trilayer-graphene/MoS_2/n-Si solar cell with a 9 nm-thick MoS_2 layer; the curves were measured under AM 1.5 illumination conditions. Photovoltaic parameters, including the open-circuit voltage V_{OC}, short-circuit current density J_{SC}, fill factor FF, and photovoltaic efficiency η, determined from this curve are indicated in the figure.

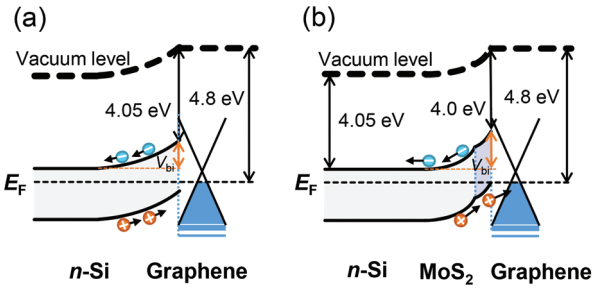

Fig. 5 Schematics of band diagrams for the solar cells. The photovoltaic processes (a) in the graphene/n-Si and (b) in the graphene/MoS_2/n-Si solar cells are shown.

hole-transporting/electron-blocking layer in the photovoltaic process, as described below in detail.

We fabricated a trilayer-graphene/MoS_2/n-Si solar cell using a thinner (~9 nm) MoS_2 film. Fig. 4 shows the J–V curve for the graphene/MoS_2/n-Si solar cell. The optimized graphene/MoS_2/n-Si solar cells exhibit V_{OC}, J_{SC}, and FF photovoltaic parameters of 0.56 V, 33.4 mA cm^{-2}, and 0.60, respectively, which results in a high photovoltaic efficiency of 11.1%. This value of 11.1% is high among the reported values for solar cells containing a MoS_2 layer.[13,14] This value over 10% is also comparable to the levels of similar hetero-junction solar cells such as graphene/Si[28–31] and PEDOT:PSS/Si.[49] A thinner layer is suitable for minimizing the shadow effect by the MoS_2 layer. Moreover, the thinner MoS_2 layer forms the thicker depletion region in the Si layer without losing the role as an electron-blocking/hole-transporting layer. This improvement indicates that more photons passed through the MoS_2 and were absorbed by the Si.

To better understand the photovoltaic process, we show band alignment diagrams for the graphene/n-Si and graphene/MoS_2/n-Si solar cells, as shown in Fig. 5. Fig. 5(a) shows the band alignment of a graphene/n-Si solar cell under ambient conditions, where the graphene has been p-doped *via* the $FeCl_3$ etching process.[50–52] The photovoltaic process in the graphene/n-Si solar cells is understood by the Schottky barrier formed at the semimetal (graphene) and semiconductor (n-Si) interface. Fig. 5(b) shows a schematic band diagram for graphene/MoS_2/n-Si solar cells.[53] We confirmed that the CVD-grown MoS_2 exhibits n-type properties on the basis of the transfer characteristics of the electric double-layer transistor (ESI S6†).[54] The insertion of an MoS_2 layer into graphene/n-Si solar cells modifies the band alignment. Indeed, the photovoltaic properties are enhanced by the insertion of an MoS_2 layer, as shown in Fig. 3(a). The total built-in voltage (V_{bi}) of graphene/MoS_2/n-Si solar cells is greater than that of the graphene/n-Si solar cell because the Schottky barrier height is determined by the energy difference between the electron affinity χ_s of the semiconductor and the work function W_m of graphene, *i.e.* $W_m - \chi_s$.[55–57] The increase of the built-in field by insertion of an MoS_2 layer can directly improve the V_{OC} and the photovoltaic conversion efficiency. Moreover, because of the difference between the Fermi levels, the bottom of the conduction band and the top of the valence band of the MoS_2 layer at the interface of graphene are shifted upward, resulting in an energy barrier at the interface between MoS_2 and n-Si. The energy barrier of the MoS_2 layer functions as an effective electron blocking layer for the photogenerated electrons in the Si layer. Furthermore, in the case of the photogenerated hole, the energy barrier created by the MoS_2 layer functions as an effective hole-transport layer. The effective carrier transporting (blocking) layer of MoS_2 effectively reduces the recombination loss of carriers, which in turn results in an increase of the J_{SC}. Therefore, the MoS_2 layer between the graphene and n-Si contributes to the enhancement of photovoltaic performance as a carrier transporting (blocking) layer, as shown in Fig. 3(a).

Conclusions

In summary, we investigated the considerable enhancement of the photovoltaic performance of graphene/Si solar cells using MoS_2. The large-area CVD-grown MoS_2 films enabled the fabrication of graphene/MoS_2/n-Si solar cells. The MoS_2 acts as an effective hole-transporting/electron-blocking layer. These contribute to the remarkable conversion efficiency of 11.1% in the fabricated trilayer-graphene/MoS_2/n-Si solar cells. The results provide a new opportunity for the application of MoS_2 thin films in various photovoltaic applications.

Materials and methods

The Raman spectrum of the MoS_2 films was obtained using a laser Raman microscope (Nanophoton, RAMANtouch). The optical absorption spectrum of the MoS_2 films on the glass substrates was recorded using a UV/Vis spectrophotometer (SHIMADZU, UV-1800). XPS was conducted on a TRXPS spectrometer (JEOL, JPS-9010TRX). The surface morphologies were measured by AFM (Agilent Technologies, 5500 Scanning

Probe Microscope). To test the photovoltaic performance, the solar cells were irradiated using a solar simulator (San-Ei Electric, XES-40S1) under AM 1.5 conditions (100 mW cm^{-2}) and the current density–voltage data were recorded using a source meter (Keithley, 2400). The AM 1.5 conditions for the solar simulator were confirmed using a standard cell (BUNKOUKEIKI, BS-500BK). For the incident-to-photon conversion efficiency (IPCE) measurements, the devices were tested using a monochromated xenon arc light system (BUNKOUKEIKI, SMO-250III).

Acknowledgements

Part of this work was supported by M. Endo, A. Wakamiya, Y. Murata, T. Nakata, and T. Morii for experimental equipment. We also thank Nitto Denko Corporation for providing us with thermal release tape. This study was supported by a Grant-in-Aid for Scientific Research from the Japan Society for Promotion of Science (Grant Nos. 26107522, 15K13500, 24681031, 25400324, 25246010, 25610074, 25000003), the Precursory Research for Embryonic Science and Technology program from the Japan Science and Technology Agency, the Yazaki Memorial Foundation for Science and Technology, the Nippon Sheet Glass Foundation for Materials Science and Engineering, and The Canon Foundation. KF acknowledges the Leading Graduate Program in Science and Engineering, Waseda University from MEXT, Japan.

Notes and references

1 A. K. Geim and K. S. Novoselov, The Rise of Graphene, *Nat. Mater.*, 2007, **6**, 183–191.
2 A. Splendiani, L. Sun, Y. Zhang, T. Li, J. Kim, C.-Y. Chim, G. Galli and F. Wang, Emerging Photoluminescence in Monolayer MoS_2, *Nano Lett.*, 2010, **10**, 1271–1275.
3 B. Radisavljevic, A. Radenovic, J. Brivio, V. Giacometti and A. Kis, Single-layer MoS_2 Transistors, *Nat. Nanotechnol.*, 2011, **6**, 147–150.
4 C. N. R. Rao, A. K. Sood, K. S. Subrahmanyam and A. Govindaraj, Graphen, Das Neue Zweidimensionale Nanomaterial, *Angew. Chem., Int. Ed.*, 2009, **121**, 7890–7916.
5 Z. He, Y. Sheng, Y. Rong, G.-D. Lee, J. Li and J. H. Warner, Layer-Dependent Modulation of Tungsten Disulfide Photoluminescence by Lateral Electric Fields, *ACS Nano*, 2015, **9**, 2740–2748.
6 Y. Saito and Y. Iwasa, Ambipolar Insulator-to-Metal Transition in Black Phosphorus by Ionic-Liquid Gating, *ACS Nano*, 2015, **9**, 3192–3198.
7 S. Li, Y. Luo, W. Lv, W. Yu, S. Wu, P. Hou, Q. Yang, Q. Meng, C. Liu and H. M. Cheng, Vertically Aligned Carbon Nanotubes Grown on Graphene Paper as Electrodes in Lithium-Ion Batteries and Dye-Sensitized Solar Cells, *Adv. Energy Mater.*, 2011, **1**, 486–490.
8 D.-M. Sun, M. Y. Timmermans, Y. Tian, A. G. Nasibulin, E. I. Kauppinen, S. Kishimoto, T. Mizutani and Y. Ohno, Flexible High-Performance Carbon Nanotube Integrated Circuits, *Nat. Nanotechnol.*, 2011, **6**, 156–161.
9 J. A. Wilson and A. D. Yoffe, The Transition Metal Dichalcogenides Discussion and Interpretation of the Observed Optical, Electrical and Structural Properties, *Adv. Phys.*, 1969, **18**, 193–335.
10 K. F. Mak, C. Lee, J. Hone, J. Shan and T. F. Heinz, Atomically Thin MoS_2: A New Direct-Gap Semiconductor, *Phys. Rev. Lett.*, 2010, **105**, 136805.
11 L. Chu, H. Schmidt, J. Pu, S. Wang, B. Özyilmaz, T. Takenobu and G. Eda, Charge Transport in Ion-Gated Mono-, Bi-, and Trilayer MoS_2 Field Effect Transistors, *Sci. Rep.*, 2014, **4**, 7293.
12 A. R. Beal, J. C. Knights and W. Y. Liang, Transmission Spectra of Some Transition Metal Dichalcogenides. II. Group VIA: Trigonal Prismatic Coordination, *J. Phys. C: Solid State Phys.*, 1972, **5**, 3540.
13 M.-L. Tsai, S.-H. Su, J.-K. Chang, D.-S. Tsai, C.-H. Chen, C.-I. Wu, L.-J. Li, L.-J. Chen and J.-H. He, Monolayer MoS_2 Heterojunction Solar Cells, *ACS Nano*, 2014, **8**, 8317–8322.
14 M. Shanmugam, C. A. Durcan and B. Yu, Layered Semiconductor Molybdenum Disulfide Nanomembrane Based Schottky-Barrier Solar Cells, *Nanoscale*, 2012, **4**, 7399–7405.
15 C. R. Dean, A. F. Young, I. Meric, C. Lee, L. Wang, S. Sorgenfrei, K. Watanabe, T. Taniguchi, P. Kim and K. L. Shepard, Boron Nitride Substrates for High-Quality Graphene Electronics, *Nat. Nanotechnol.*, 2010, **5**, 722–726.
16 Y. Yoon, K. Ganapathi and S. Salahuddin, How Good Can Monolayer MoS_2 Transistors Be?, *Nano Lett.*, 2011, **11**, 3768–3773.
17 H. Wang, L. Yu, Y.-H. Lee, Y. Shi, A. Hsu, M. L. Chin, L.-J. Li, M. Dubey, J. Kong and T. Palacios, Integrated Circuits Based on Bilayer MoS_2 Transistors, *Nano Lett.*, 2012, **12**, 4674–4680.
18 Z. Yin, H. Li, H. Li, L. Jiang, Y. Shi, Y. Sun, G. Lu, Q. Zhang, X. Chen and H. Zhang, Single-Layer MoS_2 Phototransistors, *ACS Nano*, 2011, **6**, 74–80.
19 K. Roy, M. Padmanabhan, S. Goswami, T. P. Sai, G. Ramalingam, S. Raghavan and A. Ghosh, Graphene-MoS_2 Hybrid Structures for Multifunctional Photoresponsive Memory Devices, *Nat. Nanotechnol.*, 2013, **8**, 826–830.
20 W. Zhang, C.-P. Chuu, J.-K. Huang, C.-H. Chen, M.-L. Tsai, Y.-H. Chang, C.-T. Liang, Y.-Z. Chen, Y.-L. Chueh and J.-H. He, Ultrahigh-Gain Photodetectors Based on Atomically Thin Graphene-MoS_2 Heterostructures, *Sci. Rep.*, 2014, **4**, 3826.
21 K. Roy, M. Padmanabhan, S. Goswami, T. P. Sai, S. Kaushal and A. Ghosh, Optically Active Heterostructures of Graphene and Ultrathin MoS_2, *Solid State Commun.*, 2013, **175**, 35–42.
22 C.-C. Chen, M. Aykol, C.-C. Chang, A. F. J. Levi and S. B. Cronin, Graphene-Silicon Schottky Diodes, *Nano Lett.*, 2011, **11**, 1863–1867.
23 X. Li, H. Zhu, K. Wang, A. Cao, J. Wei, C. Li, Y. Jia, Z. Li, X. Li and D. Wu, Graphene-on-Silicon Schottky Junction Solar Cells, *Adv. Mater.*, 2010, **22**, 2743–2748.

24 C. Xie, P. Lv, B. Nie, J. Jie, X. Zhang, Z. Wang, P. Jiang, Z. Hu, L. Luo and Z. Zhu, Monolayer Graphene Film/Silicon Nanowire Array Schottky Junction Solar Cells, *Appl. Phys. Lett.*, 2011, **99**, 133113.

25 K. Cui, A. S. Anisimov, T. Chiba, S. Fujii, H. Kataura, A. G. Nasibulin, S. Chiashi, E. I. Kauppinen and S. Maruyama, Air-Stable High-Efficiency Solar Cells with Dry-Transferred Single-Walled Carbon Nanotube Films, *J. Mater. Chem. A*, 2014, **2**, 11311–11318.

26 F. Wang, D. Kozawa, Y. Miyauchi, K. Hiraoka, S. Mouri, Y. Ohno and K. Matsuda, Fabrication of Single-walled Carbon Nanotube/Si Heterojunction Solar Cells with High Photovoltaic Conversion Performance, *ACS Photonics*, 2014, **1**, 360–364.

27 K.-S. Behuraa, S. Nayaka, I. Mukhopadhyayb and O. Jania, Junction Characteristics of Chemically-derived Graphene/p-Si Heterojunction Solar Cell, *Carbon*, 2014, **67**, 766–774.

28 X. Miao, S. Tongay, M. K. Petterson, K. Berke, A. G. Rinzler, B. R. Appleton and A. F. Hebard, High Efficiency Graphene Solar Cells by Chemical Doping, *Nano Lett.*, 2012, **12**, 2745–2750.

29 X. Li, D. Xie, H. Park, M. Zhu, T. H. Zeng, K. Wang, D. Wei, J. Kong and H. Zhu, Ion Doping of Graphene for High-Efficiency Heterojunction Solar Cells, *Nanoscale*, 2013, **5**, 1945–1948.

30 T. Cui, R. Lv, Z.-H. Huang, S. Chen, Z. Zhang, X. Gan, Y. Jia, X. Li, K. Wang and D. Wu, Enhanced Efficiency of Graphene/Silicon Heterojunction Solar Cells by Molecular Doping, *J. Mater. Chem. A*, 2013, **1**, 5736–5740.

31 L. Yang, X. Yu, M. Xu, H. Chen and D. Yang, Interface Engineering for Efficient and Stable Chemical-Doping-Free Graphene-on-Silicon Solar Cells by Introducing a Graphene Oxide Interlayer, *J. Mater. Chem. A*, 2014, **2**, 16877–16883.

32 E. Shi, H. Li, L. Yang, L. Zhang, Z. Li, P. Li, Y. Shang, S. Wu, X. Li and J. Wei, Colloidal Antireflection Coating Improves Graphene-Silicon Solar Cells, *Nano Lett.*, 2013, **13**, 1776–1781.

33 X. Liu, X. W. Zhang, Z. G. Yin, J. H. Meng, H. L. Gao, L. Q. Zhang, Y. J. Zhao and H. L. Wang, Enhanced Efficiency of Graphene-Silicon Schottky Junction Solar Cells by Doping with Au Nanoparticles, *Appl. Phys. Lett.*, 2014, **105**, 183901.

34 Y. Song, X. Li, C. Mackin, X. Zhang, W. Fang, T. Palacios, H. Zhu and J. Kong, Role of Interfacial Oxide in High-Efficiency Graphene-Silicon Schottky Barrier Solar Cells, *Nano Lett.*, 2015, **15**, 2104–2110.

35 F. Wang, D. Kozawa, Y. Miyauchi, K. Hiraoka, S. Mouri, Y. Ohno and K. Matsuda, Considerably Improved Photovoltaic Performance of Carbon Nanotube-Based Solar Cells Using Metal Oxide Layers, *Nat. Commun.*, 2015, **6**, 6305.

36 Y. Zhan, Z. Liu, S. Najmaei, P. M. Ajayan and J. Lou, Large-Area Vapor-Phase Growth and Characterization of MoS_2 Atomic Layers on a SiO_2 Substrate, *Small*, 2012, **8**, 966–971.

37 Y. H. Lee, X. Q. Zhang, W. Zhang, M. T. Chang, C. T. Lin, K. D. Chang, Y. C. Yu, J. T. W. Wang, C. S. Chang and L. J. Li, Synthesis of Large-Area MoS_2 Atomic Layers with Chemical Vapor Deposition, *Adv. Mater.*, 2012, **24**, 2320–2325.

38 J. Wu, H. Schmidt, K. K. Amara, X. Xu, G. Eda and B. Özyilmaz, Large Thermoelectricity via Variable Range Hopping in Chemical Vapor Deposition Grown Single-Layer MoS_2, *Nano Lett.*, 2014, **14**, 2730–2734.

39 A. Reina, H. Son, L. Jiao, B. Fan, M. S. Dresselhaus, Z. Liu and J. Kong, Transferring and Identification of Single- and Few-Layer Graphene on Arbitrary Substrates, *J. Phys. Chem. C*, 2008, **112**, 17741–17744.

40 H. Li, J. Wu, X. Huang, Z. Yin, J. Liu, H. Zhang and A. Universal, Rapid Method for Clean Transfer of Nanostructures onto Various Substrates, *ACS Nano*, 2014, **8**, 6563–6570.

41 H. Li, Q. Zhang, C. C. R. Yap, B. K. Tay, T. H. T. Edwin, A. Olivier and D. Baillargeat, From Bulk to Monolayer MoS_2: Evolution of Raman Scattering, *Adv. Funct. Mater.*, 2012, **22**, 1385–1390.

42 C. Lee, H. Yan, L. E. Brus, T. F. Heinz, J. Hone and S. Ryu, Anomalous Lattice Vibrations of Single- and Few-Layer MoS_2, *ACS Nano*, 2010, **4**, 2695–2700.

43 D. Kozawa, R. Kumar, A. Carvalho, K. K. Amara, W. Zhao, S. Wang, M. Toh, R. M. Ribeiro, A. C. Neto, K. Matsuda and G. Eda, Photocarrier Relaxation Pathway in Two-Dimensional Semiconducting Transition Metal Dichalcogenides, *Nat. Commun.*, 2014, **5**, 4543.

44 A. Carvalho, R. M. Ribeiro and A. H. C. Neto, Band Nesting and the Optical Response of Two-Dimensional Semiconducting Transition Metal Dichalcogenides, *Phys. Rev. B: Condens. Matter*, 2013, **88**, 115205.

45 R. F. Frindt, Single Crystals of MoS_2 Several Molecular Layers Thick, *J. Appl. Phys.*, 1966, **37**, 1928–1929.

46 Y. Zhang, Y. Sun and B. Zhong, Synthesis of Higher Alcohols from Syngas over Ultrafine Mo-Co-K Catalysts, *Catal. Lett.*, 2001, **76**, 249–253.

47 L. Benoist, D. Gonbeau, G. Pfister-Guillouzo, E. Schmidt, G. Meunier and A. Levasseur, XPS Analysis of Lithium Intercalation in Thin Films of Molybdenum Oxysulphides, *Surf. Interface Anal.*, 1994, **22**, 206–210.

48 S. Bae, H. Kim, Y. Lee, X. Xu, J.-S. Park, Y. Zheng, J. Balakrishnan, T. Lei, H. R. Kim and Y. I. Song, Roll-To-Roll Production of 30-Inch Graphene Films for Transparent Electrodes, *Nat. Nanotechnol.*, 2010, **5**, 574–578.

49 J.-Y. Chen, M.-H. Yu, S.-F. Chang and K.-W. Sun, Highly Efficient Poly(3,4-ethylenedioxythiophene):poly(styrenesulfonate)/Si Hybrid Solar Cells with Imprinted Nanopyramid Structures, *Appl. Phys. Lett.*, 2013, 103.

50 D. Zhan, L. Sun, Z. H. Ni, L. Liu, X. F. Fan, Y. Wang, T. Yu, Y. M. Lam, W. Huang and Z. X. Shen, $FeCl_3$-Based Few-Layer Graphene Intercalation Compounds: Single Linear Dispersion Electronic Band Structure and Strong Charge Transfer Doping, *Adv. Funct. Mater.*, 2010, **20**, 3504–3509.

51 W. Zhang, C.-T. Lin, K.-K. Liu, T. Tite, C.-Y. Su, C.-H. Chang, Y.-H. Lee, C.-W. Chu, K.-H. Wei and J.-L. Kuo, Opening an Electrical Band Gap of Bilayer Graphene with Molecular Doping, *ACS Nano*, 2011, **5**, 7517–7524.

52 S. Ryu, L. Liu, S. Berciaud, Y.-J. Yu, H. Liu, P. Kim, G. W. Flynn and L. E. Brus, Atmospheric Oxygen Binding and Hole Doping in Deformed Graphene on a SiO_2 Substrate, *Nano Lett.*, 2010, **10**, 4944–4951.
53 S. Behura and V. Berry, Interfacial Nondegenerate Doping of MoS_2 and Other Two-dimensional Semiconductors, *ACS Nano*, 2015, **9**, 2227–2230.
54 J. Pu, Y. Yomogida, K.-K. Liu, L.-J. Li, Y. Iwasa and T. Takenobu, Highly Flexible MoS_2 Thin-Film Transistors with Ion Gel Dielectrics, *Nano Lett.*, 2012, **12**, 4013–4017.
55 S. Das, H.-Y. Chen, A. V. Penumatcha and J. Appenzeller, High Performance Multilayer MoS_2 Transistors with Scandium Contacts, *Nano Lett.*, 2012, **13**, 100–105.
56 D. Fu, J. Zhou, S. Tongay, K. Liu, W. Fan, T.-J. K. Liu and J. Wu, Mechanically Modulated Tunneling Resistance in Monolayer MoS_2, *Appl. Phys. Lett.*, 2013, **103**, 183105.
57 Y.-J. Yu, Y. Zhao, S. Ryu, L. E. Brus, K. S. Kim and P. Kim, Tuning the Graphene Work Function by Electric Field Effect, *Nano Lett.*, 2009, **9**, 3430–3434.